



Published in final edited form as:

Ann Biomed Eng. 2020 March ; 48(3): 1103–1111. doi:10.1007/s10439-020-02453-9.

Design of an Adhesive Film-Based Microfluidic Device for Alginate Hydrogel-Based Cell Encapsulation

Kevin Enck^{1,2}, Shiny Priya Rajan^{1,2}, Julio Aleman¹, Simone Castagno³, Emily Long⁴, Fatma Khalil¹, Adam R. Hall^{1,2}, Emmanuel C. Opara^{1,2}

¹Wake Forest Institute for Regenerative Medicine, Wake Forest School of Medicine, Medical Center Boulevard, Winston-Salem, NC 27157, USA

²Virginia Tech-Wake Forest School of Biomedical Engineering and Sciences, Wake Forest School of Medicine, Medical Center Boulevard, Winston-Salem, NC 27157, USA

³Imperial College London, Kensington, London SW7 2AZ, UK

⁴Wake Forest Institute for Regenerative Medicine Summer Undergraduate Research Program, Wake Forest School of Medicine, Medical Center, Winston-Salem, NC 27157, USA

Abstract

To support the increasing translational use of transplanted cells, there is a need for high-throughput cell encapsulation technologies. Microfluidics is a particularly promising candidate technology to address this need, but conventional polydimethylsiloxane devices have encountered challenges that have limited their utility, including clogging, leaking, material swelling, high cost, and limited scalability. Here, we use a rapid prototyping approach incorporating patterned adhesive thin films to develop a reusable microfluidic device that can produce alginate hydrogel microbeads with high-throughput potential for microencapsulation applications. We show that beads formed in our device have high sphericity and monodispersity. We use the system to demonstrate effective cell encapsulation of mesenchymal stem cells and show that they can be maintained in culture for at least 28 days with no measurable reduction in viability. Our approach is highly scalable and will support diverse translational applications of microencapsulated cells.

Keywords

Alginate; Microencapsulation; Stem cell; Cell transplantation

INTRODUCTION

The use of microfluidic devices (MFDs) to incorporate cells into synthetic matrices has become increasingly popular over the past two decades. For example, cells mixed

Address correspondence to Emmanuel C. Opara, Wake Forest Institute for Regenerative Medicine, Wake Forest School of Medicine, Medical Center Boulevard, Winston-Salem, NC 27157, USA. eopara@wakehealth.edu.

ELECTRONIC SUPPLEMENTARY MATERIAL

The online version of this article (<https://doi.org/10.1007/s10439-020-02453-9>) contains supplementary material, which is available to authorized users.

with hydrogel precursor can be introduced to fluid channels where gelation dynamics and device configuration can then be used to produce cell-laden layers or constructs. The resulting structures have been employed subsequently for applications like drug delivery^{21,40,53,57} and 3D cell culture studies.^{18,60,66,67} An emerging MFD approach that has taken particular advantage of the unique fluid mechanics in small scale channels has been droplet encapsulation. Here, cells are encased in discrete beads of aqueous media formed dynamically using a hydrophobic compound like mineral oil as an emulsifier.^{23,46} The system is amenable to high-throughput production and the size and composition of the resulting droplets can be engineered for applications ranging from cell sorting and screening to diverse analytical assessments.^{3,7,13,14,19,42,44,48,57} Critically, the approach also enables simple collection and transfer of encapsulated cells for downstream translational applications.

While many hydrogels can be employed for MFD droplet encapsulation, alginate is a common choice because it is bioinert and cross-links rapidly when exposed to divalent cations. In addition, alginate microbeads have also been shown to immunisolate cells *in vivo* when paired with specific polymers like poly-L-lysine or poly-L-ornithine.^{17,32,37} Consequently, it is used broadly in the field, with a notable example being islet encapsulation for diabetes treatment.^{17,29,32,37} A major practical challenge to the gelation of alginate beads in a MFD is the difficulty with which divalent cations (Ca^{2+}) can be introduced to the precursor beads through the immiscible oil surrounding them. One solution to this challenge has involved suspending CaCO_3 nanoparticles in the alginate that can then be decomposed with low pH to release calcium locally for gelation.^{2,31,50,63,65} However, this approach results in heterogeneous cross-linking due to inconsistent nanoparticle dispersion, causing bead instability and limiting downstream application. In response, an alternative method to address the challenge was reported by Utech *et al.*⁵⁸ in which calcium-ethylenediaminetetraacetic acid (Ca-EDTA) was instead introduced to the alginate. Similar to the nanoparticles, Ca-EDTA could be dissociated with reduced pH to release Ca^{2+} for cross-linking, but as a small molecule, could be dispersed more homogeneously in the alginate to promote more complete gelation.

Despite the success of Ca-EDTA for generating alginate beads in a MFD, obstacles remain to its broad utilization. For example, the approach has been implemented only in conventional polydimethylsiloxane (PDMS) MFDs which are prone to clogging and leaking due to internal gelation.^{2,50,63,65} In this report, we circumvent these challenges by implementing an unconventional material and channel design. For this, we employ an adhesive film-based MFD strategy that has low infrastructure requirements while still being able to produce microbeads with size and shape similar to PDMS devices. Most PDMS devices have utilized a slow “pinch off” mechanism to form hydrogel beads.^{10,22,23,36,59} As an additional improvement, we also produce alginate beads in the jetting regime^{8,23,36,43} in our adhesive-film MFDs, through which formation by Rayleigh-Plateau instabilities (RPIs) greatly increases throughput. This phenomenon is not new to MFD droplet production and is actually employed in droplet production outside of MFDs, and such as electrospinning.^{24,54,64} RPI defines how a jet of fluid is broken into a steady stream of droplets through perturbations and vibrations that are inherent to every stream of liquid.⁶ To assess our approach, we focus on four key alginate bead formation properties that are critical

to translation: throughput, monodispersity, size, and sphericity.^{50,58} While many device designs sacrifice throughput to maximize the remaining three characteristics, we show that our system retains high throughput, through RPI, while yielding beads with reproducible and controllable profiles. We subsequently demonstrate the utility of the approach for effective cell encapsulation using mesenchymal stem cells (MSCs) as a model system, showing high viability for at least 28 days. These results, enabled by a system that is easily scalable and more reusable than PDMS devices, will enhance translation of alginate-encapsulated cells for clinical applications. While RPI has been used previously for rapid droplet production,^{1,26,38,62} there is no report, to our knowledge, of cell encapsulation within monodisperse crosslinked hydrogels under the jetting regime. While this may be a narrow classification, there are many downstream applications that require cells to be encapsulated in small, monodisperse, and rapidly produced hydrogel constructs.

MATERIALS AND METHODS

Reagents and Materials

The water-immiscible carrier fluid is made by mixing mineral oil with 1% (v/v) Tween-80 (P4780, Sigma-Aldrich). A 50 mM concentration of the Ca-EDTA cross-linker solution is formed by mixing 100 mM CaCl₂ (C77, Fisher Scientific) with an equal volume of 100 mM EDTA (E-5134, Sigma-Aldrich). Ultrapure LVM alginate (BP-1312-29, Novamatrix, Sandvika, Norway) is mixed in a 1.5% (w/v) solution with the 50 mM Ca-EDTA solution and kept on ice prior to use. The low-pH cross-link initiator solution is made by mixing mineral oil with 1.4% (v/v) acetic acid (0714, Amresco).

Device Fabrication

MFDs are fabricated from adhesive thin films using a low-cost laser cutting technique for rapid prototyping. Adhesive film patterning has a resolution (typically ~ 100 μm) that is sufficient for cell encapsulation applications while eliminating the need for the clean room facilities and mask aligners used in PDMS-based device production.^{4,15} In addition, the fabrication approach is rapid and adaptable, produces highly stable devices, and does not require use of a prefabricated master. The MFD consists of four layers: a glass base, the microfluidic layer, a lid layer featuring inlets/outlets, and a top PDMS layer to prevent leaks (Fig. 1a). The microfluidic layer comprises an adhesive film (9495MPF, 3M, Minneapolis, MN) patterned by CO₂ laser cutting (Full Spectrum, Las Vegas, NV) and attached to a glass microscope slide. Channel thickness can be varied up to several millimeters using multiple film layers, but for this report, all devices consist of a single 100 μm thick layer. The lid layer consists of a 3 mm thick PMMA sheet (McMaster-Carr, Douglasville, GA), a 4 mm thick PDMS layer (10:1 Sylgard 184, Dow Corning Corporation, Midland, MI), and two adhesive film layers between the two. Inlets and outlets are formed in the PDMS layer with a 20G blunt needle and in the PMMA and adhesive film layers by CO₂ laser cutting. The top surface of the PMMA is attached to one adhesive film and subsequently sealed to the bottom surface of the PDMS using air plasma to improve bonding strength. The entire lid layer is then placed on the top surface of the patterned microfluidic layer to form the closed MFD. The resulting device is sealed by applying even pressure to the entire device. Polytetrafluoroethylene (PTFE, Cole-Parmer, Vernon Hills, IL) tubing is

inserted into each port for fluid delivery and the MFD is left overnight at room temperature for proper sealing of the adhesive film.

Microbead Formation

The MFD (Fig. 1) consists of three inlets (i, ii, and iii) and one outlet (iv). The mineral oil and cross-linking fluids are introduced through inlets (i) and (iii), respectively, using a microfluidic syringe pump (Braintree Scientific, Braintree, MA). Once the channels are filled with oil, the 1.5% alginate–Ca–EDTA solution is introduced through inlet (ii), forming droplets upon contact with the immiscible mineral oil (Fig. 1b, left inset). Further downstream in the channel, the droplets are cross-linked due to decreased pH induced by the acetic acid–mineral oil mixture (Fig. 1b, right inset). The ensuing sinusoidal segment of the channel is used to promote full mixing of the carrier and acetic acid–oil mixtures through induction of turbulent flow, thereby releasing Ca^{2+} in the beads and cross-linking them. Microbeads are collected in a 50 mL conical tube connected to the (iv) port by tubing. Excess oil is aspirated from the solution before washing with hexane three times, letting the beads settle each time before aspirating, and adding fresh hexane to the microbead pellet. The hexane dissolves the residual mineral oil, allowing for effective transfer from the organic phase to aqueous media. The beads are finally washed with 100 mM CaCl_2 three times to (1) ensure proper gelation, (2) return the pH to 7.4, and (3) remove any excess hexane as it has been shown to be cytotoxic over an extended period of time. The material can be used immediately or stored in 25 mM CaCl_2 at 4 °C.

SEM Imaging

Alginate microbeads made from the MFD were collected and washed according to the previous method above. Liquid alginate was then carefully poured onto the beads and crosslinked with 100 mM CaCl_2 for 5 min. The larger alginate structure was then carefully dehydrated with gradually increasing concentrations of ethanol (50–100%). The beads were critical point dried then imaged with a FlexSEM 1000.

Cell Culture and Encapsulation

Bone marrow-derived MSCs are cultured with DMEM (PT-3238, Lonza) at 37 °C and 5% CO_2 in T-175 flasks (Ref 431080, Corning) until confluent. Cells are trypsinized, centrifuged, washed, and then mixed with the Ca–EDTA–alginate solution at a concentration of 1.5×10^6 cells/mL. The alginate-cell mixture is employed to produce beads *via* the same protocol that was used for clean alginate above. Following encapsulation, cell-laden beads are cultured in DMEM in 6 well plates (08–772-33, Fisher) at a cell concentration of about 1.0×10^5 mL²¹ for up to 28 days. Viability is determined on days 0, 3, 7, 14, 21, and 28 *via* a LIVE–DEAD assay (Vybrant CFDA, Invitrogen) in which carboxyfluorescein diacetate (CFDA) is used to stain living cells and propidium iodide (PI) is used to stain dead cells.

Inverted Microscope Imaging

All images are taken with a Zeiss Axiovert 200M inverted microscope. Quantitative image analysis is performed using ImageJ software.⁴¹ Bead production rates are determined from videos over set timeframes of approximately 3 s per condition.

RESULTS

Many previous cell-encapsulation MFDs operate using a dripping mechanism,^{2,11,22,23,27,30,31,36,46,47,51,52,56,58,59,61,65} in which beads are formed one at a time due to periodic droplet necking by fluid surface tension. We employ RPI as a mechanism to produce beads.^{23,36,43,56} Through this effect, minor friction-induced perturbations in the outer surface of a coaxial fluid thread amplify until they eventually form the thread into droplets. Because this instability is an intrinsic feature of a fluid jet, tunable droplet formation can occur in rapidly flowing conditions with very high frequency.

A critical factor for encapsulation devices is the achievable rate of bead production. Dripping regime MFDs conventionally have very low throughput^{10,23,36,55,56} because of the slow, serial manner in which beads are formed. This ultimately limits their translational utility by limiting yield, making higher rates strongly beneficial. We therefore next assess how the bead production rate varies with the key experimental parameter of W_f . We initially evaluate the operation of a MFD with a narrow channel downstream of the alginate–oil junction (Supplementary Fig. S1) that promotes a dripping mechanism of bead formation. Here, we maintain a constant mineral oil flow rate (4 mL/h) and vary that of the alginate. Note that the different device geometry prevents a direct quantitative comparison of these results to the W_f of our RPI device above, but values are similar and the results provide a valuable counterpoint. As shown in Fig. 2a, the dripping MFD achieves a bead production rate of typically 5–10 s⁻¹ with no discernible dependence on W_f across the investigated range. This rate is similar to that of other dripping MFDs previously published, with some even claiming to be high-throughput.⁵⁶ In contrast, bead formation *via* the RPI mechanism (Fig. 2b) yields a rate 10–15 times higher than that of the conventional dripping MFD with a strong, linear dependence on W_f . This demonstrates the increased throughput attainable with the RPI mechanism as well as the reproducibility of the device as this was performed across multiple devices ($n = 3$) of the same pattern.

We next produce cross-linked alginate beads under various flow conditions to determine the variability and the controllability of RPI formation. Figure 3 shows a histogram for beads produced using an example condition along with the bright field image from which the measurement are obtained (inset). We observe a narrow Gaussian population of diameter. Table 1 shows data collected across five experimental conditions for which we maintain the flow rate of carrier fluid (mineral oil) at a constant 100 μ L/h. For convenience and for direct comparison to previous literature,³⁵ we consider as a parameter the water fraction²⁵ W_f , defined as

$$W_f = \frac{V_w}{(V_w + V_o)}, \quad (1)$$

where V_w is the volumetric flow rate of the aqueous (alginate) stream and V_o is that of the carrier fluid. For these purposes, the W_f is the ratio of volume of alginate following through the device compared to the total volume of all fluids flowing through the device. Since

the oil and alginate flow rate are both changing due to optimization, having one parameter to track them both simplifies the analytical comparisons. For quantitation, bead size and shape are determined through analysis of bright-field micrographs with three parameters considered in particular: diameter D , aspect ratio R , and circularity C . D is determined from the total area ($\pi D^2/4$) of each bead measured from an image. R is calculated as the ratio of the major axis to the minor axis while C is expressed simply as:

$$C = 4\pi \left(\frac{A}{P^2} \right), \quad (2)$$

where P is bead perimeter measured from the image. For both R and C , values approaching 1.0 are indicative of greater bead sphericity. In Fig. 4, an SEM image of an alginate bead created by the MFD is shown. This image visually demonstrates the sphericity and smoothness of the beads. Although there is debris around the beads, this is thought to be due to the alginate surrounding the beads, and it was unavoidable to capture them during imaging. In addition, we also consider the coefficient of variance (CV) as a metric of monodispersity, defined as the ratio of the standard deviation of bead diameter to its mean. Generally, a population is considered to be monodisperse when CV is less than 5%.

We observe that beads are formed under all investigated conditions and find that bead diameter generally increases with increasing W_f , in agreement with past work.³⁵ Across the entire examined range, we achieve high values for both C (0.82 – 0.89) and R (0.96 – 1.04) with no apparent dependence on W_f . While there may be conditions that don't lead to the creation of such round beads, this data indicates that there is a wide range of parameters that produce spherical microcapsules. Because large beads are known to induce inflammation and/or immunogenic responses²⁰ that would limit the efficacy of cell transplantation applications, beads with small D and low CV are essential. For minimal D , low W_f is preferred. We note that the determination of D is a projection from a 2D image obtained inside the MFD. While the precise diameters of beads produced at higher W_f in our system may be skewed somewhat by the 100 μm chamber thickness, the measured value can be considered the largest bead dimension. In addition, while monodisperse or nearly-monodisperse beads are observed over nearly the entire range, we find dramatically larger CV values for W_f at or below 0.010 in our system. Therefore, despite the reduced attainable diameter, low W_f are inadequate. As a result, from these data we identify $W_f = 0.012$ as the optimal condition for RPI bead formation in our MFD, producing consistent, circular beads with small diameter at a high rate.

Having established the ability to produce highly regular and spherical microbeads at high production rates, we next incorporate cells in the alginate solution to perform cell encapsulation. To demonstrate this, we employ bone marrow-derived MSCs and quantify viability over a 28 day culture using a custom Matlab code (see Supplementary Information). Figures 5a–5e show typical images of encapsulated cells with LIVE–DEAD stain at all time points where green indicates live cells and red indicates dead cells. We

observe consistently high MSC viability approaching 100% across the entire investigated range, similar to that obtained in traditional 2D culture (Fig. 5f). Note that because of the change in pH associated with cross-linking (see “Materials and Methods”), it is particularly important to show that the cells remain viable after the encapsulation process itself, as confirmed by the data. High cell viability is thus maintained for at least 28 days in the microbeads produced by our MFD, demonstrating the biocompatible nature of the encapsulation process. Conversely, these results also demonstrate that the addition of cells to the alginate does not prevent gelation.

DISCUSSION

As cell therapy gains momentum, the need will arise for encapsulated cells to be transplanted directly into tissue. Microencapsulation in polymeric hydrogels—including alginate with perm-selective coatings^{12,28}—enables the immunoisolation and localization of allogeneic cells for clinical applications. For example, MSCs like those employed here can potentially supply sustained release of therapeutic molecules to provide localized immune tolerance that may be beneficial for treating auto-immune diseases.^{5,34,45} MFDs for cell encapsulation have significant potential to achieve success *in vivo* based on four key characteristics: bead size, monodispersity, sphericity, and production throughput. For bead size, smaller diameters allow for better nutrient diffusion^{50,58} and reduce inflammatory responses in tissue.²⁰ Similarly, high monodispersity limits the number of beads with diameter outside the target size range while also enabling more accurate dosing of cells for therapeutic applications; a critical factor when millions of beads are being produced. We found that monodispersity became worse as the W_f dropped below 0.010 and this is most likely due to the RPI phenomena. As the oil flow rate increases, which decreases the W_f , the droplet formation becomes more rapid, but eventually the alginate droplets are formed too chaotically leading to a higher polydispersity in diameter. High-sphericity beads have a decreased risk for macrophage and protein attachment, thus minimizing inflammatory response as well.¹⁶ Finally, greater throughput enables the rapid production of large quantities of cell-laden beads, which will be essential to translational dissemination. Many cell therapies involve transplantation of concentrations over 1×10^6 cells/mL in order to see clinical success.^{33,39,49} The beads have finite space available to the cells, so increasing droplet production is the only way to create a therapeutically relevant volume of beads. Hypothetically, if 30 cells were encapsulated in each bead and the production rate was 100 beads/s, it would take less than 6 min to encapsulate 1×10^6 cells. The number of cells able to fit in each microbead varies highly between cell types and bead size so investigators will need to determine this independently. Spherical, monodisperse beads that are less than 200 μm in diameter are typically made with MFDs.^{2,31,47,50,58} However, there is currently a limited availability of methods that are capable of producing these beads in a relatively high throughput due to the conventional reliance on the dripping mechanism of encapsulation. While highly controlled, this method forms beads serially, after which they typically travel single file along the MFD, introducing a bottleneck to translational applications.

In this report, we employ a RPI mechanism to generate small diameter beads with high sphericity and monodispersity in a higher-throughput manner than previous MFDs. The large opening in our device immediately after the alginate–oil junction (see Fig. 1b) provides

a rapid reduction in fluid velocity that promotes jetting instability, ultimately leading to droplet formation through a RPI mechanism. While increasing the throughput up to 10–15-fold compared to dripping regime devices, we are still able to produce beads with properties that are potentially constructive for translational applications. For example, under our optimal conditions, we demonstrate formation of alginate beads with D of $89.72 \pm 2.49 \mu\text{m}$, C of 0.86 ± 0.09 , and a CV of 2.77%. Once formed, our beads are then introduced to acidic mineral oil to reduce pH and promote the release of Ca^{2+} from Ca–EDTA and cross-link the alginate homogeneously. Critically, we also demonstrate that these beads are capable of supporting cells to maintain viability in long-term culture. Using bone marrow-derived MSCs as a model cell type, we show efficient incorporation into MFD-produced beads. The cells can be maintained for at least 28 days post-encapsulation with no significant reduction in viability observed, suggesting their utility for downstream applications.

While a single device may not be able to encapsulate clinically-relevant volumes of cells, our MFD can be scaled easily, run in parallel, and quickly adapted due to the use of rapid prototyping with adhesive film microfluidics. We have also found that with proper maintenance and cleaning, our devices can be used up to five times before any apparent reduction in bead production quality. This reduction comes from gradual build-up of alginate and oil at the edges and junctions of the device. In contrast, conventional PDMS devices are typically capable of only a single use due to the narrow size of the channels which tend to be the same size as the beads they produce.^{9,14,27} Meanwhile, our device has much larger channels which allows for droplets to flow around beads that get stuck, thus improving reusability. PDMS devices also require a new master (and thus photomask) to be produced for each different MFD design, potentially limiting experimental throughput.²³ Therefore, our approach has significant potential to enhance the translational use of encapsulated MSCs for regenerative medicine applications.

Supplementary Material

Refer to Web version on PubMed Central for supplementary material.

ACKNOWLEDGMENTS

The authors would like to acknowledge the support of Michael Hunckler, Michael LeCompte, and Paige Brabant for their technical help on this project. K.E. acknowledges support from the NIH T32 Training Program entitled Studies in Translational Regenerative Medicine (EB014836-01A1).

REFERENCES

1. Abate AR, Kutsovsky M, Seiffert S, Windbergs M, Pinto LF, Rotem A, Utada AS, and Weitz DA. Synthesis of monodisperse microparticles from non-Newtonian polymer solutions with microfluidic devices. *Adv. Mater.* 23(15):1757–1760, 2011. [PubMed: 21394794]
2. Akbari S, and Pirbodaghi T. Microfluidic encapsulation of cells in alginate particles via an improved internal gelation approach. *Microfluid. Nanofluid.* 16(4):773–777, 2014.
3. Andersson H, and Van den Berg A. Microfluidic devices for cellomics: a review. *Sens. Actuators B* 92(3):315–325, 2003.
4. Atencia J, Cooksey GA, and Locascio LE. A robust diffusion-based gradient generator for dynamic cell assays. *Lab Chip* 12(2):309–316, 2012. [PubMed: 22113489]

5. Boura JS, Vance M, Yin W, Madeira C, Da Silva CL, Porada CD, and Almeida-Porada G. Evaluation of gene delivery strategies to efficiently overexpress functional HLA-G on human bone marrow stromal cells. *Mol. Ther. Methods Clin. Dev.* 2014. 10.1038/mtm.2014.41.
6. Breslouer O Rayleigh–Plateau Instability: Falling Jet. Project Report. 2010.
7. Chabert M, and Viovy J-L. Microfluidic high-throughput encapsulation and hydrodynamic self-sorting of single cells. *Proc. Natl Acad. Sci. USA* 105(9):3191–3196, 2008. [PubMed: 18316742]
8. Chaurasia AS, and Sajjadi S. Millimetric core–shell drops via buoyancy assisted non-confined microfluidics. *Chem. Eng. Sci.* 129:260–270, 2015.
9. Choi C-H, Jung J-H, Rhee YW, Kim D-P, Shim S-E, and Lee C-S. Generation of monodisperse alginate microbeads and in situ encapsulation of cell in microfluidic device. *Biomed. Microdevices* 9(6):855–862, 2007. [PubMed: 17578667]
10. Christopher GF, Noharuddin NN, Taylor JA, and Anna SL. Experimental observations of the squeezing-to-dripping transition in T-shaped microfluidic junctions. *Phys. Rev. E* 78(3):036317, 2008.
11. Chung BG, Lee K-H, Khademhosseini A, and Lee S-H. Microfluidic fabrication of microengineered hydrogels and their application in tissue engineering. *Lab Chip* 12(1):45–59, 2012. [PubMed: 22105780]
12. Cirone P, Shen F, and Chang PL. A multiprong approach to cancer gene therapy by coencapsulated cells. *Cancer Gene Ther.* 12(4):369, 2005. [PubMed: 15692610]
13. Clausell-Tormos J, Lieber D, Baret J-C, El-Harrak A, Miller OJ, Frenz L, Blouwolff J, Humphry KJ, Köster S, and Duan H. Droplet-based microfluidic platforms for the encapsulation and screening of mammalian cells and multicellular organisms. *Chem. Biol.* 15(5):427–437, 2008. [PubMed: 18482695]
14. Collins DJ, Neild A, deMello A, Liu A-Q, and Ai Y. The Poisson distribution and beyond: methods for microfluidic droplet production and single cell encapsulation. *Lab Chip* 15(17):3439–3459, 2015. [PubMed: 26226550]
15. Cooksey GA, and Atencia J. Pneumatic valves in folded 2D and 3D fluidic devices made from plastic films and tapes. *Lab Chip* 14(10):1665–1668, 2014. [PubMed: 24691845]
16. De Vos P, De Haan B, Wolters G, Strubbe J, and Van Schilfgaarde R. Improved biocompatibility but limited graft survival after purification of alginate for microencapsulation of pancreatic islets. *Diabetologia* 40(3):262–270, 1997. [PubMed: 9084963]
17. de Vos P, Faas MM, Strand B, and Calafiore R. Alginate-based microcapsules for immunoisolation of pancreatic islets. *Biomaterials* 27(32):5603–5617, 2006. [PubMed: 16879864]
18. Dvir-Ginzberg M, Elkayam T, and Cohen S. Induced differentiation and maturation of newborn liver cells into functional hepatic tissue in macroporous alginate scaffolds. *FASEB J.* 22(5):1440–1449, 2008. [PubMed: 18070820]
19. Edd JF, Di Carlo D, Humphry KJ, Köster S, Irimia D, Weitz DA, and Toner M. Controlled encapsulation of single-cells into monodisperse picolitre drops. *Lab Chip* 8(8):1262–1264, 2008. [PubMed: 18651066]
20. Gelb H, Ralph Schumacher H, Cuckler J, and Baker DG. In vivo inflammatory response to polymethylmethacrylate particulate debris: effect of size, morphology, and surface area. *J. Orthop. Res.* 12(1):83–92, 1994. [PubMed: 8113946]
21. Gombotz WR, and Wee S. Protein release from alginate matrices. *Adv. Drug Deliv. Rev.* 31(3):267–285, 1998. [PubMed: 10837629]
22. Huang K-S, Lai T-H, and Lin Y-C. Manipulating the generation of Ca–alginate microspheres using microfluidic channels as a carrier of gold nanoparticles. *Lab Chip* 6(7):954–957, 2006. [PubMed: 16804602]
23. Huang H, Yu Y, Hu Y, He X, Usta OB, and Yarmush ML. Generation and manipulation of hydrogel microcapsules by droplet-based microfluidics for mammalian cell culture. *Lab Chip* 17(11):1913–1932, 2017. [PubMed: 28509918]
24. Jayasinghe SN, Qureshi AN, and Eagles PA. Electrohydrodynamic jet processing: an advanced electric-field-driven jetting phenomenon for processing living cells. *Small* 2(2):216–219, 2006. [PubMed: 17193023]

25. Jenkins G, and Mansfield CD. *Microfluidic Diagnostics: Methods and Protocols*. Cham: Springer, 2013.
26. Jing T, Ramji R, Warkiani ME, Han J, Lim CT, and Chen C-H. Jetting microfluidics with size-sorting capability for single-cell protease detection. *Biosens. Bioelectron.* 66:19–23, 2015. [PubMed: 25460876]
27. Köster S, Angile FE, Duan H, Agresti JJ, Wintner A, Schmitz C, Rowat AC, Merten CA, Pisignano D, and Griffiths AD. Drop-based microfluidic devices for encapsulation of single cells. *Lab Chip* 8(7):1110–1115, 2008. [PubMed: 18584086]
28. Krishnamurthy N, and Gimi B. Encapsulated cell grafts to treat cellular deficiencies and dysfunction. *Crit. Rev. Biomed. Eng.* 2011. 10.1615/critrevbiomedeng.v39.i6.10.
29. Lee KY, and Mooney DJ. Alginate: properties and biomedical applications. *Prog. Polym. Sci.* 37(1):106–126, 2012. [PubMed: 22125349]
30. Liu K, Deng Y, Zhang N, Li S, Ding H, Guo F, Liu W, Guo S, and Zhao X-Z. Generation of disk-like hydrogel beads for cell encapsulation and manipulation using a droplet-based microfluidic device. *Microfluid. Nanofluid.* 13(5):761–767, 2012.
31. Martinez CJ, Kim JW, Ye C, Ortiz I, Rowat AC, Marquez M, and Weitz D. A microfluidic approach to encapsulate living cells in uniform alginate hydrogel microparticles. *Macromol. Biosci.* 12(7):946–951, 2012. [PubMed: 22311460]
32. McQuilling J, Arenas-Herrera J, Childers C, Pareta R, Khanna O, Jiang B, Brey E, Farney A, and Opara E. New alginate microcapsule system for angiogenic protein delivery and immunoisolation of islets for transplantation in the rat omentum pouch. *Transplant. Proc.* 43:3262–3264, 2011. [PubMed: 22099771]
33. Meier RP, Mahou R, Morel P, Meyer J, Montanari E, Muller YD, Christofilopoulos P, Wandrey C, Gonelle-Gispert C, and Bühler LH. Microencapsulated human mesenchymal stem cells decrease liver fibrosis in mice. *J. Hepatol.* 62(3):634–641, 2015. [PubMed: 25450712]
34. Nasef A, Mathieu N, Chapel A, Frick J, François S, Mazurier C, Boutarfa A, Bouchet S, Gorin N-C, and Thierry D. Immunosuppressive effects of mesenchymal stem cells: involvement of HLA-G. *Transplantation* 84(2):231–237, 2007. [PubMed: 17667815]
35. Ngo I-L, Dang T-D, Byon C, and Joo SW. A numerical study on the dynamics of droplet formation in a microfluidic double T-junction. *Biomicrofluidics* 9(2):024107, 2015. [PubMed: 25825622]
36. Nunes J, Tsai S, Wan J, and Stone H. Dripping and jetting in microfluidic multiphase flows applied to particle and fibre synthesis. *J. Phys. D* 46(11):114002, 2013.
37. Opara EC, McQuilling JP, and Farney AC. Microencapsulation of pancreatic islets for use in a bioartificial pancreas. In: *Organ Regeneration: Methods and Protocols*, edited by Basu J, and Ludlow JW. Totowa, NJ: Humana Press, 2013, pp. 261–266.
38. Pessi J, Santos HA, Miroshnyk I, Weitz DA, and Mirza S. Microfluidics-assisted engineering of polymeric microcapsules with high encapsulation efficiency for protein drug delivery. *Int. J. Pharm.* 472(1–2):82–87, 2014. [PubMed: 24928131]
39. Ponticciello MS, Schinagl RM, Kadiyala S, and Barry FP. Gelatin-based resorbable sponge as a carrier matrix for human mesenchymal stem cells in cartilage regeneration therapy. *J. Biomed. Mater. Res. Off. J. Soc. Biomater. Jpn. Soc. Biomater. Aust. Soc. Biomater. Korean Soc. Biomater.* 52(2):246–255, 2000.
40. Ramdas M, Dileep K, Anitha Y, Paul W, and Sharma CP. Alginate encapsulated bioadhesive chitosan microspheres for intestinal drug delivery. *J. Biomater. Appl.* 13(4):290–296, 1999. [PubMed: 10340211]
41. Rasband WS ImageJ. Bethesda, MD: US National Institutes of Health, 2011. <http://imagej.nih.gov/ij/>.
42. Sajeesh P, and Sen AK. Particle separation and sorting in microfluidic devices: a review. *Microfluid. Nanofluid.* 17(1):1–52, 2014.
43. Sauret A, and Shum HC. Beating the jetting regime. *Int. J. Nonlinear Sci. Numer. Simul.* 13(5):351–362, 2012.
44. Schmitz CH, Rowat AC, Köster S, and Weitz DA. Dropspots: a picoliter array in a microfluidic device. *Lab Chip* 9(1):44–49, 2009. [PubMed: 19209334]

45. Selmani Z, Naji A, Gaiffe E, Obert L, Tiberghien P, Rouas-Freiss N, Carosella ED, and Deschaseaux F. HLA-G is a crucial immunosuppressive molecule secreted by adult human mesenchymal stem cells. *Transplantation* 87(9S):S62–S66, 2009. [PubMed: 19424010]
46. Sharma V, Hunckler M, Ramasubramanian MK, Opara EC, and Katuri KC. *Microfluidic approach to cell microencapsulation*, New York: Springer, 2017, pp. 71–76.
47. Shintaku H, Kuwabara T, Kawano S, Suzuki T, Kanno I, and Kotera H. Micro cell encapsulation and its hydrogel-beads production using microfluidic device. *Microsyst. Technol.* 13(8–10):951–958, 2007.
48. Sia SK, and Whitesides GM. Microfluidic devices fabricated in poly (dimethylsiloxane) for biological studies. *Electrophoresis* 24(21):3563–3576, 2003. [PubMed: 14613181]
49. Sittadjody S, Saul JM, McQuilling JP, Joo S, Register TC, Yoo JJ, Atala A, and Opara EC. In vivo transplantation of 3D encapsulated ovarian constructs in rats corrects abnormalities of ovarian failure. *Nat. Commun.* 8(1):1858, 2017. [PubMed: 29208899]
50. Tan WH, and Takeuchi S. Monodisperse alginate hydrogel microbeads for cell encapsulation. *Adv. Mater.* 19(18):2696–2701, 2007.
51. Tendulkar S, McQuilling J, Childers C, Pareta R, Opara E, and Ramasubramanian M. A scalable microfluidic device for the mass production of microencapsulated islets. *Transplant. Proc.* 43:3184–3187, 2011. [PubMed: 22099752]
52. Tendulkar S, Ramasubramanian MK, and Opara EC. Microencapsulation: the emerging role of microfluidics. *Micro Nanosyst.* 5(3):194–208, 2013.
53. Tønnesen HH, and Karlsen J. Alginate in drug delivery systems. *Drug Dev. Ind. Pharm.* 28(6):621–630, 2002. [PubMed: 12149954]
54. Townsend-Nicholson A, and Jayasinghe SN. Cell electrospinning: a unique biotechnique for encapsulating living organisms for generating active biological microthreads/scaffolds. *Biomacromolecules* 7(12):3364–3369, 2006. [PubMed: 17154464]
55. Trivedi V, Ereifej ES, Doshi A, Sehgal P, VandeVord PJ, and Basu AS. Microfluidic encapsulation of cells in alginate capsules for high throughput screening. In: 2009 Annual International Conference of the IEEE Engineering in Medicine and Biology Society. IEEE, 2009, pp. 7037–7040.
56. Utada A, Chu L-Y, Fernandez-Nieves A, Link D, Holtze C, and Weitz D. Dripping, jetting, drops, and wetting: the magic of microfluidics. *MRS Bull.* 32(9):702–708, 2007.
57. Utada A, Lorenceau E, Link D, Kaplan P, Stone H, and Weitz D. Monodisperse double emulsions generated from a microcapillary device. *Science* 308(5721):537–541, 2005. [PubMed: 15845850]
58. Utech S, Prodanovic R, Mao AS, Ostafe R, Mooney DJ, and Weitz DA. Microfluidic generation of monodisperse, structurally homogeneous alginate microgels for cell encapsulation and 3D cell culture. *Adv. Healthc. Mater.* 4(11):1628–1633, 2015. [PubMed: 26039892]
59. Velasco D, Tumarkin E, and Kumacheva E. Microfluidic encapsulation of cells in polymer microgels. *Small* 8(11):1633–1642, 2012. [PubMed: 22467645]
60. Venkatesan J, Bhatnagar I, Manivasagan P, Kang K-H, and Kim S-K. Alginate composites for bone tissue engineering: a review. *Int. J. Biol. Macromol.* 72:269–281, 2015. [PubMed: 25020082]
61. Whitesides GM The origins and the future of microfluidics. *Nature* 442(7101):368, 2006. [PubMed: 16871203]
62. Windbergs M, Zhao Y, Heyman J, and Weitz DA. Biodegradable core–shell carriers for simultaneous encapsulation of synergistic actives. *J. Am. Chem. Soc.* 135(21):7933–7937, 2013. [PubMed: 23631388]
63. Workman VL, Dunnett SB, Kille P, and Palmer DD. On-chip alginate microencapsulation of functional cells. *Macromol. Rapid Commun.* 29(2):165–170, 2008.
64. Workman VL, Tezera LB, Elkington PT, and Jayasinghe SN. Controlled generation of microspheres incorporating extracellular matrix fibrils for three-dimensional cell culture. *Adv. Funct. Mater.* 24(18):2648–2657, 2014. [PubMed: 25411575]
65. Xu J, Li S, Tan J, and Luo G. Controllable preparation of monodispersed calcium alginate microbeads in a novel microfluidic system. *Chem. Eng. Technol. Ind. Chem. Plant Equip. Process Eng. Biotechnol.* 31(8):1223–1226, 2008.

66. Yamada M, Utoh R, Ohashi K, Tatsumi K, Yamato M, Okano T, and Seki M. Controlled formation of heterotypic hepatic micro-organoids in anisotropic hydrogel microfibers for long-term preservation of liver-specific functions. *Biomaterials* 33(33):8304–8315, 2012. [PubMed: 22906609]
67. Yang Y, Opara EC, Liu Y, Atala A, and Zhao W. Microencapsulation of porcine thyroid cell organoids within a polymer microcapsule construct. *Exp. Biol. Med.* 242(3):286–296, 2017.

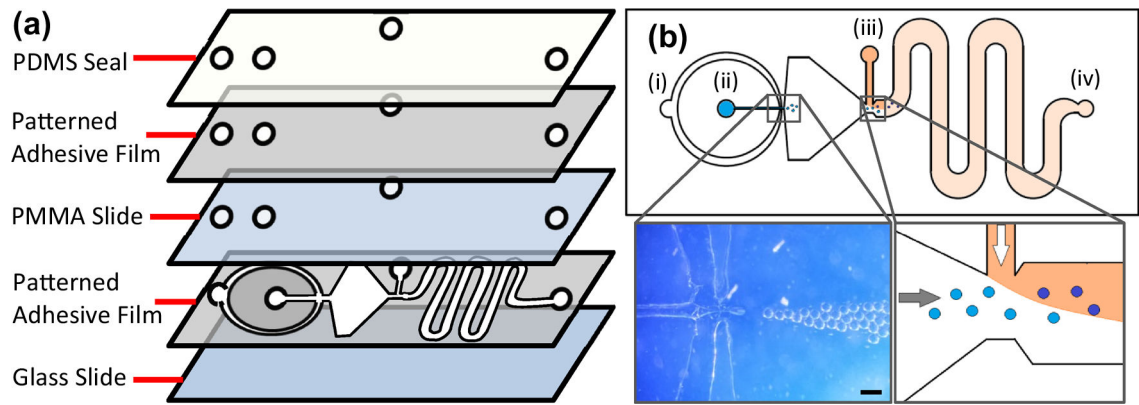


FIGURE 1.

MFD design. (a) Layered view of MFD. The adhesive film is patterned, attached to the glass slide, and then covered with a PMMA/PDMS seal. The PDMS forms a tight junction with the tubing to prevent leakage. (b) (i) Mineral oil inlet, (ii) alginate-Ca-EDTA inlet, (iii) acetic acid-mineral oil inlet, (iv) collection outlet. Left inset: magnified optical image showing high throughput bead formation. Scale bar is 150 μm . Right inset: schematic showing introduction of acetic acid-mineral oil (orange) to reduce solution pH and cross-link the alginate beads homogeneously through release of Ca^{2+} from the Ca-EDTA.

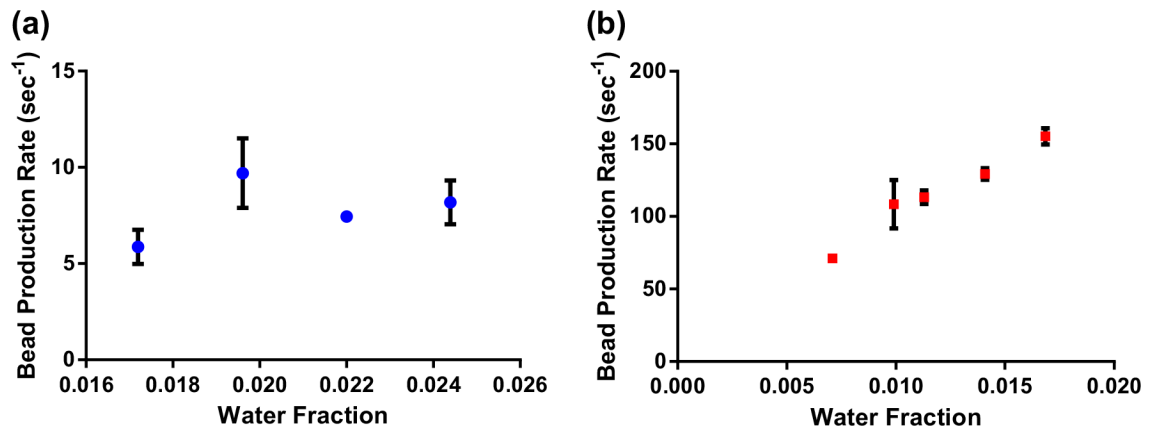


FIGURE 2. Bead production rate as a function of W_f in dripping regime (a) and RPI (b) devices. Data was collected on multiple independent MFDs for most W_f conditions ($n = 3$).

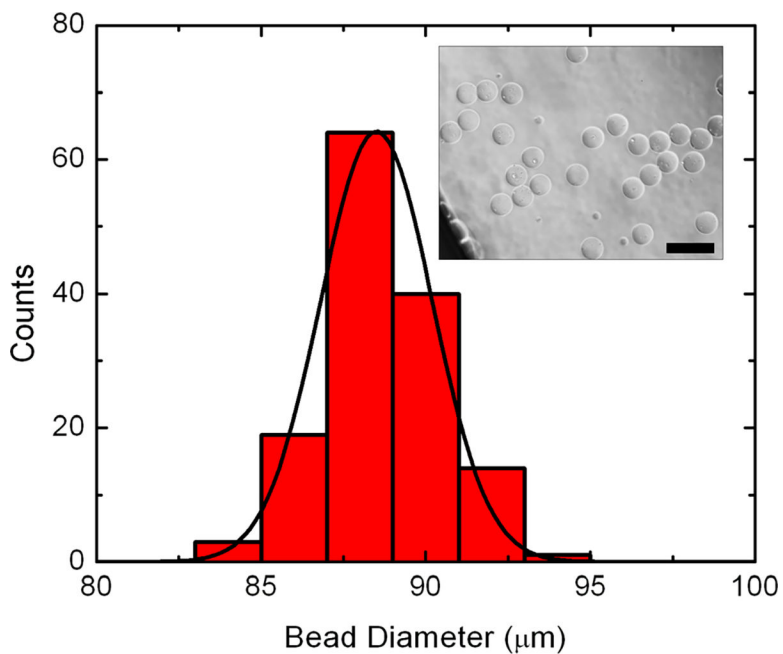


FIGURE 3.

Histogram of alginate bead diameter for flow rate conditions of 8, 100, and 8 mL/h supplied to inlets (i), (ii), and (iii) channel respectively. Black line is a Gaussian fit to the data, indicating an average microbead size of $89.72 \mu\text{m}$. $n = 141$. Inset: example bright-field optical micrograph of beads produced with the described condition. Analysis of such images provides the quantitative results used in the histogram as well as the other parameters described in the text. Scale bar is $100 \mu\text{m}$.

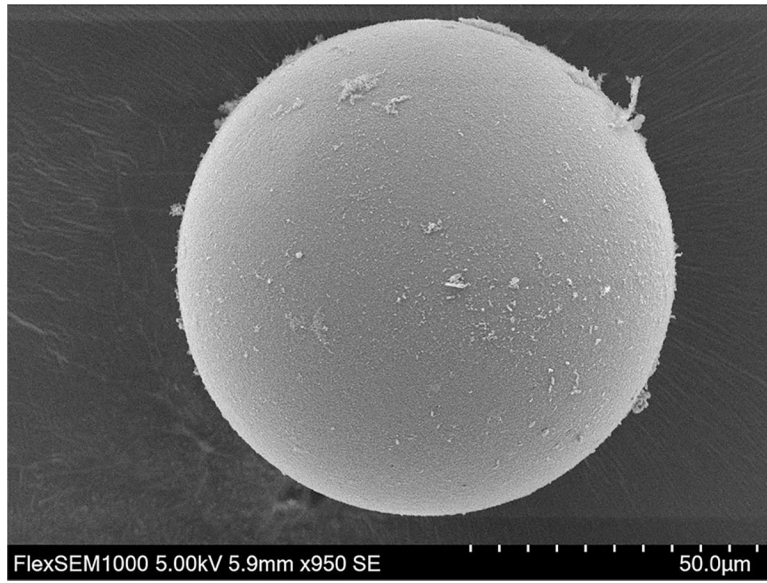


FIGURE 4. SEM image of alginate microbead made with MFD. Beads sphericity and smoothness is shown in high resolution. The debris seen around the bead is most likely due to the alginate that was used to trap the beads after they were crosslinked. The scale bar and magnification can be seen in the bottom bar.

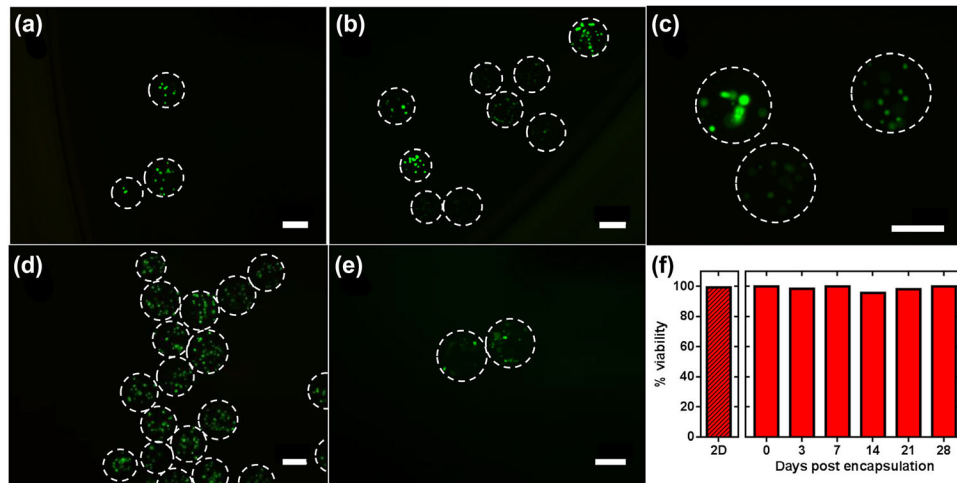


FIGURE 5.

Example fluorescent micrographs showing LIVE–DEAD staining of encapsulated MSCs 0 (a); 3 (b); 7 (c); 14 (d); and 28 (e) days after encapsulation. Day 21 data is shown in Supplementary Fig. S2. Dashed lines are bead outlines determined from bright-field images of the same sample. Green indicates live cells and red indicates dead cells. All scale bars are 100 μm . (f) Viability of MSCs across all investigated time points. Datum labeled 2D represents viability in conventional 2D cell culture before encapsulation and day 0 represents viability directly following encapsulation.

TABLE 1.

Alginate microbead properties as a function of oil flow rate through channel (i).

Flow Rate _i (mL/h)	W_r	D (μm)	C	R	CV (%)
3	0.032	180.65 \pm 7.42	0.85 \pm 0.07	0.96 \pm 0.02	4.11
4	0.024	124.51 \pm 6.37	0.82 \pm 0.10	1.04 \pm 0.03	5.12
6	0.016	131.53 \pm 4.94	0.89 \pm 0.07	0.98 \pm 0.02	3.76
8	<i>0.012</i>	<i>89.72 \pm 2.49</i>	<i>0.86 \pm 0.09</i>	<i>1.03 \pm 0.02</i>	<i>2.77</i>
14	0.007	54.84 \pm 9.63	0.83 \pm 0.12	0.95 \pm .03	17.6

Alginate flow rate (ii) is kept constant at 100 $\mu\text{L}/\text{h}$. Flow rate of acetic acid–oil (iii) is downstream and does not impact results. The optimal condition identified for our system is in italics. From T-B, $n = 38$, 68, 51, 141, and 193 respectively.